International Journal of Research in Advanced Engineering and Technology
www.allengineeringjournal.in
ISSN: 2455-0876
Received: 20-02-2024, Accepted: 14-03-2024, Published: 05-04-2024
Volume 10, Issue 1, 2024, Page No. 5-12

Simultaneous adsorptive removal of Pb^{2+}, Cu^{2+} and phenol from wastewater: Kinetics and equilibrium behavior

Agbale N R[1], Agarry S E[2], Ogunleye O O[2], Arinkoola A O[3]
[1] Lecturer, Deparment of Chemical Engineer, Delta State University, Abraka, Oleh Campus, Nigeria
[2] Professor, Deparment of Chemical Engineer, Ladoke Akintola University of Technology, Ogbomosho, Nigeria
[3] Reader, Deparment of Chemical Engineer, Ladoke Akintola University of Technology, Ogbomosho, Nigeria

Abstract
Wastewater is oftentimes, a cocktail of pollutants that need to be simultaneously removed at optimal efficiencies. In this study, novel green tri-composites biochar (T-BC) of kaolin, plantain pseudo stem and snail shell were synthesized at 500, 600 and 700 ^{o}C for the simultaneous adsorption of Pb^{2+}, Cu^{2+} and phenol. The T-BC at 500 ^{o}C performed best, and was employed in further studies of the adsorption efficiencies. The pseudo first order model gave the best fit for the kinetic data of phenol, while those of Pb^{2+} and Cu^{2+} were best fitted to the pseudo second-order model in the multi-polluted system (MPS). The MPS equilibrium data for Pb^{2+} was well correlated to the modified competitive Langmuir and Langmuir models, the non-modified competitive Langmuir and Freundlich gave good fits for the data of Cu^{2+} and the Sheindorf–Rebuhn–Sheintuch (SRS) model and Freundlich models gave the best fit for the adsorption of phenol. The Freundlich model gave the best correlation for the adsorption of Pb^{2+}, Cu^{2+} and phenol in the single polluted system. The maximum adsorption capacities in the MPS were 25.22, 98.69 and 151.45mg/g; 382.84, 627.95 and 225.19 mg/g; and 382.82, 1449.21 and 8503.28 mg/g for Pb^{2+}. Cu^{2+} and phenol respectively using the Langmuir, MCL and NMCL isotherms. The presence of pollutants resulted in the synergy of the adsorption process. The adsorption process was endothermic, spontaneous and feasible for all of the pollutants at 25, 35 and 45 ^{o}C. The T-BC showed great potential for the adsorption of HMS and organics.

Keywords: Adsorption, multi-polluted water, green adsorbent, modified isotherms

Introduction

Water pollution which is the major cause of water shortage ensues mostly from the activities of man, coupled with increasing population growth. Wastewater discharged from mining, extractive, textile, agricultural, petroleum refining is composed of heavy metals (HMS) and organic at concentrations higher than the allowable limits for discharge into surface water (Jianga *et al*.,2020 [6]. These pollutants are highly toxic, affecting human health and the environment adversely. HMS are not biodegradable thus, they accumulate in water bodies, soils and humans (Zhang *et al*., 2023) [24]. Exposure to HMS causes respiratory dysfunctions, and irritate the skin, while long-term exposures results in life-threatening disease as cancer and kidney disorders (Paithankar *et al*., 2021) [12]. A high concentration of phenol in wastewater could lead to improper assimilation of protein which causes the breakdown of tissues, and failure of the nervous system, kidney, liver and pancreatic tissues. This has necessitated researches on the removal of these HM and organics. Nonetheless, most researches have been in the treatment of the single-component polluted water, and these are not adaptable to practical situations, in which wastewater is made up of pollutants that interact with each other to affect the sorption process (Yadav *et al*., 2021 [20]; Jeppu *et al*., 2023) It becomes imperative, therefore to develop cheap and sustainable materials and process that will simultaneously remove these co-existing pollutants effectively.

Adsorption, an interfacial process is preferred to other methods of environmental remediation such as membrane separation, coagulation, ion exchange and precipitation due to its flexible design, cheap operational cost, fast removal of pollutants, non-generation of secondary pollutants (Arif *et al*., 2021) [1]. Adsorbents that are synthesized from natural materials such as plant biomass, clay minerals and animal wastes have been studied immensely because they are easily accessible, cheap and they promote green technology (Premarathna *et al*., 2019) [15]

Clay minerals have been used extensively in the development of clay-biochar composites to improve their mechanical strength and porosity (Wang *et al*., 2019) [19]. CaCO3-containing minerals are another class of cheap and abundant minerals used for the remediation of the environment due to their porous structures, high ash and alkali metal contents which enhance its adsorptive properties in environmental remediation (Zhang *et al*., 2021) [22]. The biogenic form of $CaCO_3$ which is found mostly in the exo- and endo- skeletons of animals have not been greatly explored. Biochar composites are effective in the removal of HM and organics from water (Nhung *et al*., 2023) [10]. Their properties are improved upon when they are used in the synthesis of composites for environmental remediation Studies have also shown that the combination of two or more materials produces composite adsorbents, better products with properties that have been enhanced, as compared to the properties of the individual components are realized. The efficiency, functionalities and specificity of the adsorbent are therefore improved (Belhouchat *et al*., 2017) [2].

In this work, tri-composite biochar (T-BC) which was composed of kaolin, plantain pseudo stem (PPS) and snail shell (SS) of the African giant snail (*Achatina achatina*) were prepared at three different temperatures of 500, 600 and 700 ^{o}C. These T-BC were characterized and their effectiveness in the simultaneous removal of PB^{2+}, Cu^{2+} and phenol were studied to determine the most effective T-BC,

which was further used to conduct other adsorption studies. pH and time were used to determine the optimum adsorption conditions, and the adsorption behaviours were determined by the kinetics and equilibrium models. The extended Langmuir and Freundlich isotherms models were applied in the evaluation of the isotherm models for multi-polluted system (MPS) and compared with the isotherm models for single-component adsorption in the MPS and single-polluted systems (SPS).

Materials and Methods

1. Materials

Kaolin, PPS and SS were used as precursors for the synthesis of T-EB Kaolin was obtained from Freedom Group of Companies, Benin City, Nigeria, while the PPS and SS were obtained as agricultural and household wastes respectively all from Benin City, Nigeria. The chemicals used are HCL, NaOH, Pb $(NO_3)_2$, $Cu(NO_3)_2{\cdot}6H_2O$, and phenol. All chemicals and reagents used were of analytical grade produced by Sigma Aldrich Chemical Company, UK, and difAlpha Chemika, Mumbai.

2. Preparation of T-BC

The PPS and SS were thoroughly washed with distilled water, then they were separately dried in an oven at 95 ^{C} for 24. They were then reduced by a pulverize to particle sizes of 20 -50µm. The T-BC was prepared by methods employed by (Yao *et al*., 2014 [21]; Popoola 2019 [14]; Wang, *et al*., 2017) [18]. In summary, 10g of PSS was added to a sonicated mixture of 4g kaolin and 2g snail shell in 500 mLs of water, this was thoroughly mixed on a magnetic stirrer for 24 hours at 180-200 rpm and room temperature to achieve homogeneity.

The mixture was filtered with a Buchner funnel lined with filter paper, dried for 6 hours at 95 ^{oC,} and transferred to a crucible for pyrolysis in a muffle furnace. (PT-A1200-125L model). The conditions of the muffle furnace are a heating time of 2 hours, a heating rate of 10 ^{o}C/min and a nitrogen flow rate of. ml/min. The pyrolysis process was repeated at 500, 600 and 700 ^{o}C. The T-BCs were labeled as T-BC500, T-BC600 and T-BC700

3. Characterization of Tri-composites

The tri-composite biochar were analysed for functional groups, crystallinity, CHNS and morphology (and microstructure) using the Fourier transform infrared spectrometer (FTIR) (Perkin-Elmer, PC1600, USA), x-ray-diffraction (Bruker D2 Phaser), and LECO TGA 701) and scanning electron microscopy (SEM, FEI ESEM Quanta 200). The SEM analysis was conducted on the best-performing biochar,

4. Batch adsorption studies

The preliminary batch adsorption to determine the optimized T-BC experiments were conducted by contacting 0.1g of the adsorbent with 50 mLs of a multi-polluted solution containing 30mg/L Pb, 40mg/L Cu and 30mg/L phenol in a 100 mL Erlenmeyer flask, the flask was covered with polyethylene and was stirred on a magnetic stirrer at a speed of 350rpm and temperature of 25^{o}C. The T-BC that has the best removal efficiency was subsequently utilized for the study of the effect of pH, kinetics and the equilibrium studies of the process.

The effect of time and kinetic studies were conducted by extracting a portion of the solution contacted with 0.1g of T-EB every 30 minutes until an equilibrium concentration was reached for the removal of the adsorbates.

The edge experiments were carried out as above, but the pH of the solution were varied between 1 and 10 by adjustment with 0.1M HCL and).1 NaOH. The effect of varying initial concentrations were studied in the single-polluted and multi-polluted systems. The initial concentrations were varied from 2-7, 2 -10 and 6 to 32 mg/L for the Pb^{2+}. Cu^{2+} and phenol in SPS, while the concentrations in the MPS were varied between 1 and 35mg/L using predetermined dosages. The concentrations of the HMS were measured by Agilent atomic adsorption spectrometer (240FS AA series, USA) and that of phenol was measured using Agilent-Technologies (Little Falls, CA, USA) 6890N Network GC system, equipped with an Agilent-Technologies 5975 inert XL Mass selective detector and Agilent- Technologies 7683B series auto-injector. All the adsorption experiments were carried out in triplicates.

The adsorption capacity of biochar is calculated s:

$$q_e = (C_0 - C_e)\frac{v}{m} \quad (1)$$

he removal efficiency is given as

$$^{o}/_{o}\, R = \left(\frac{c_0 - c\mathrm{e}}{c_0}\right) \times 100 \quad (2)$$

where Co and Ce are initial and equilibrium concentrations of the pollutants (mg/L), V is the
volume of solution (L) and ma is the mass of adsorbent (g).

Results and discussions

1. Characteristics of T-BC

The CHNS results also in Table 1 indicated that carbon (C) had the highest percentage for all the T-BC at all temperatures. The C content, however, decreased with an increase in temperature. T-BC500 had the highest carbon content of 43.29%, which was reduced by 62% to 16.41 in T-BC700. This is consistent with results obtained in previous studies in which C content decreased with temperature for biochar pyrolyzed from high mineral-based precursors (Dai *et al*., 2017).

The functional group analyses are shown in Fig. 1(a). The stretches between 3650 and 3750 represent an -OH group. The peak around 2988 cm-1 was due to the $-CH_2$ bonds of aliphatic chains. The peaks at 1470 cm^{-1} to 1479 cm^{-1} could be a result of the presence of the C═C such as olefins and aromatic ring. The peaks at 1415–1410 cm^{-1} are associated with dominant C–O for tri-composites treated at above 500 ^{C}. The SS shells are composed of $CaCO_3$, so the peaks at 859 -876; 1,050 – 1,066; and 1,475 cm^{-1} belong to are due to the presence of carbonate. The presence of organic siloxane and silicate Si-C-O is represented by peaks 1030 - 1080 cm^{-1}, these bands also indicate the presence of Si-O-Al and Si-O-Mg, confirming the presence of kaolin. Peaks at 1066 and 1032 represent the presence of N-H groups found in primary amines and ammonium ions which were ascribed to the presence of conchin (Oladoja *et al*.,2015) [13] As the

pyrolysis temperature increased, the tri-composite biochar becomes less complex. The complex characteristics of the adsorbents suggest that the presence of active functional groups in the adsorbent will facilitate the uptake of pollutants onto its surface and pores (Kooh *et al*., 2015) [7]. The above evidence proved the successful synthesis of a tri-composite biochar adsorbent made up of kaolin, PPS, and SS.

The XRD patterns shown in Fig 2. indicate the presence of $CaCO_3$ at peaks 2θ = 29., 35, 39 and 47. The peaks around 31° show the presence of calcium-magnesium calcites, while the peaks between 25.6° and 26.4° affirm the presence of SiO_2 in the form of quartz.

Table 1: CHNS composition of T-EB400, T-eB500, T-Eb600 and T-EB700

Adsorbent	N	C	H	S
T-EB500	0.24	27.56	0.71	
T-EB600	0.20	19.55	0.59	
T-EB700	0.03	16.41	0.34	0.00

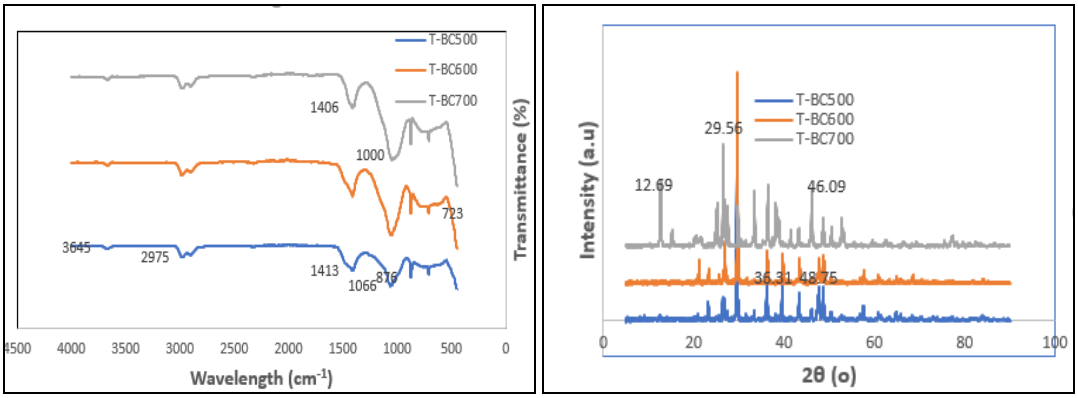

(a) (b)

Fig 1: (a) FTIR properties of T-BC (b) XRD spectra of T-BC

3. Preliminary adsorption

Table 2 shows the removal efficiency of the adsorbents in adsorbing Pb^{2+}. Cu^{2+} and phenol from a multi-polluted solution of the three pollutants. The performance of the adsorbents was nearly close, however, T-BC500 gave a better performance for the adsorption of all the pollutants with 100, 81.90, and 79.43% removal for Pb^{2+}, Cu^{2+} and phenol respectively. This would be selected for further studies, as its production would imply less cost, due to the reduced cost of energy at the lowest temperature of 500°C.

Table 2: Removal efficiency of Pb^{2+}, Cu^{2+}, and phenol on the different T-BC

Adsorbent	Cu^{-2+}	Pb	Phenol
Removal efficiency (%)			
T-BC500	91.90	100.00	79.43
T-BC600	90.92	100.00	81,02
T-BC700	89.54	100.00	72.91

4. Effect of pH

The effect of pH on the removal efficiency (RE) of $Pb^{2+}$of initial concentration 10mg/L, Cu^{2+} (20mg/L) and phenol (30mg/L) on T-BC in the MPS was conducted in the pH range of 2 and 10, at a temperature of 23°C, adsorbent dosage of 2g/L and in 60 minutes. The plots of Fig. 4 show that pH had a significant effect on the adsorption of the HMS. The RE were 11.1 to 100% for Pb^{2+}, and 8.3 to 92.56% for Cu^{2+}. The RE of the HMS gradually increased with pH up to 6, then at pH 7, a decline in the RE started to occur. The low RE at pH 2 to 4, was due to the presence of protons which compete for adsorption sites with the HMS. This phenomenon was also due to the existence of –COOH and –OH functional groups, which enables the carboxylic on the surface to remain as carboxylic (Zhang *et al*., 2023) [24]. The pH pzc of T-EB400 is 4.8 (fig. 5), which implies that the surface of the adsorbent becomes negatively charged at all pH values above 4.9, thus the adsorption of the HM onto the sites by electrostatic attraction is favoured. As the pH tends to alkalinity, the presence of OH^- ions results in the formation of metallic hydroxides precipitate which lowers the driving force of the ions, thereby leading to reduced efficiency. The RE of phenol remained constant throughout the entire range of pH due to its low degree of ionization in solution. Molecular adsorption through van der Waals forces is the controlling mechanism, for the adsorption of phenol,

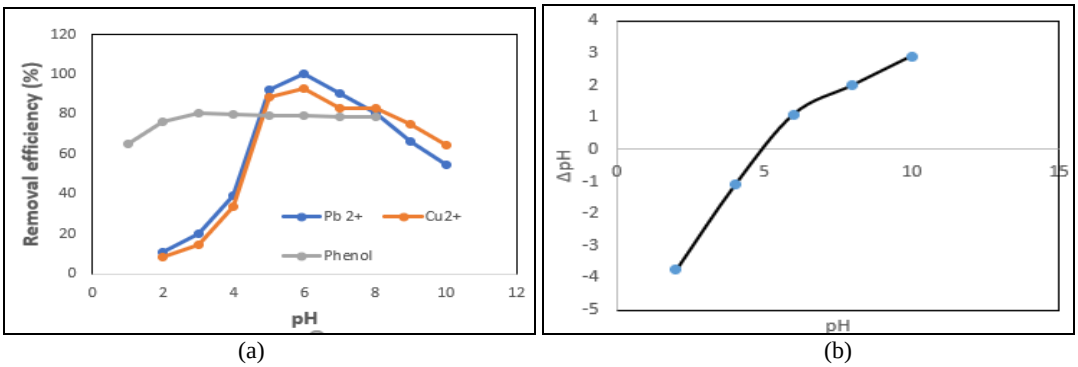

(a) (b)

Fig 2: (a). Effect of pH on the Removal Efficiency of Pb^{2+}, Cu^{2+} and phenol; (b): pH_{PZC} of T-BC500

5. Adsorption kinetics

Adsorption kinetics aid in the determination of the rate-controlling steps of the process, which is a requirement for the design of the adsorption process. The kinetic data of the simultaneous adsorption of PB^{2+}, Cu^{2+} and phenol in MPS on T-BC500 were fitted to PFO and PSO kinetic models, and the Webber-Morris intra-particle diffusion was employed in the determination of the removal mechanisms of the pollutants. The linear equations for the PFO and PSO models are represented in equations 3 and 4, while the IPD model equation is represented in equation 5. The obtained kinetic parameters and their corresponding coefficient of determination (R^2) values are provided in Table 5. The plots are presented in Fig 5(a-c).

The PFO model as developed by Lagergren for solid-liquid processes was evaluated from equation 3

$$\log(q_e - q_t) = \log q_e - \frac{k_1 t}{2 \cdot 303}$$

$$\log(q_e - q_t) vs.\, t\,. \qquad (3)$$

Equation 4 was proposed by Ho and McKay (1999) predict the PSO model (Rr. Prihatdini *et al*., 2023) [17].

$$\frac{t}{q_t} = \frac{1}{k_2 q_e^2} + \frac{t}{q_e} \qquad (4)$$

The determination of the rate-controlling mechanism as hypothesized by Webber and Morris is shown in equation 5 (Zhang *et al*., 2023) [24]

$$q_t = K_{dif} t^{0.5} + C \qquad (5)$$

where q_e and q_t (mg/g) are the amounts of substances removed from the aqueous phase by the biochar at equilibrium time and t, respectively; k_1 (hr^{-1}) and k_2 (g/(mg/min) are the PFO and PSO. rate constant. k_1, was obtained from the slope of the linear plot of $\log(q_e - q_t)$ against time, t, while the second-order sorption rate constant k_2 (g/g/min) is determined from the intercept by plotting t/qt versus time t, whereas q_e is determined from the reciprocal of the slope of the straight line and k_2 equals quotient of the square of the slope and intercept (Rr. Prihatdini *et al*., 2023) [17]. k_{dif} (mg/g·$h^{1/2}$) is the intra-particle diffusion constant; and C (mg/g) is the intercept which is a function of the thickness of the boundary layer. The intra-particle diffusion parameter, K_{dif}, were obtained from the slope of the linear plot of $q_t vs. t^{0.5}$ (Yu *et al*., 2021).

The correlation coefficient R^2 and the closeness of $qe_{(exp)}$ to qe(calc) were the criereria in determining the fitness of the experimental data to the kinetic models. The PSO model shows that qe(exp) of Pb^{2+} and Cu $^{2+}$ are 24.00 and 40.50mg/g, and the $q_{e(cal)}$ for are 24.21 and 40.08mg/L while the R^2 values are 0.9897 and 0.9772 respectively, thus confirming that the adsorption under study is more appropriately described by the PSO model.The PFO model fits the experimental data for the adsorption of phenol, with an R^2 value of 0.9952, and a $qe_{(cal)}$ value of 48.37 mg/L. which is close to the $qe_{(exp)}$ is 49.80mg/L. These results imply that the rate-controlling mechanism for the adsorption of Pb^{2+} and Cu^{2+} is chemisorption, characterised by shared or transferred electrons and that of the adsorption of phenol is physiosorption. The value of the rate constant of Pb^{2+} (k_2 = 0.002) was higher than those of Cu^{2+} (k_2 = 0.004) and phenol (k_1 = 0.0005) due to its faster rate of removal. In the assessment of the rate-determining steps depicted in Fig 4(c), it is seen that the adsorption of Pb^{2+} and Cu^{2+} occurred in three steps, while the plot for the adsorption of phenol is a straight line that does not pass through the origin. For the multi-linear curves, the first lines suggest an intr-particle diffusion while the second and third segments may likely be due to the attainment of the final equilibrium of the system. The straight line plot of phenol that does not pass through may be due to intraparticle diffusion and any or all of the following: rapid diffusion, external resistance and boundary layer effect (Touihri *et al*., 2021).

Table 3: PFO, PSO and IPD parameters of the adsorption of Pb^{2+}. Cu^{2+} and phenol on T-BC500

Pollutant/qe(exp)		PFO model			PSO model			IPD		
	$q_{e(exp)}$	K_1 (min^{-1})	$qe_{(calc)}$ (mg/g)	R^2	K_2 (g mg^{-1} min^{-1})	$qe_{(calc)}$ (mg/g)	R^2	C (mg/g)	kind (mg/g.$min^{0.5}$)	R^2
Pb^{2+}	24.00	0.03	40.11	0.8913	0.004	24.21	0.9897	93.78	12.53	0.8806
Cu^{2+}	40.50	0.04	59.08	0.8758	0.002	40.18	0.9772	27.63	5.76	0/7287
Phenol	49.80	0.0005	48.37	0.9986	0.0003	98.86	0.7175	48.55	10.21	0.9969

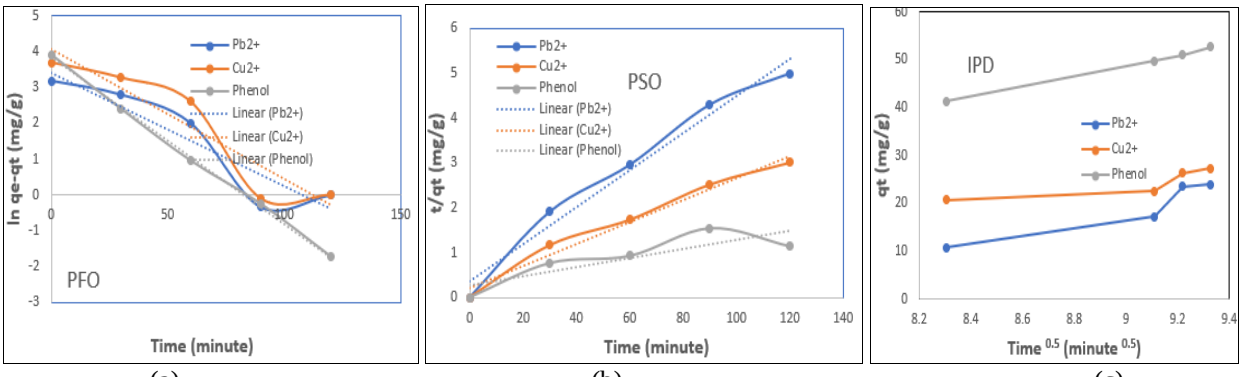

(a) (b) (c)

Fig 3: Linearized kinetics for the adsorption of Pb^{2+}, Cu^{2+} -and phenol on T-BC500 (a). PFO; (b). PSO. (c) IPD model

3.6. Isotherm models of the adsorption processes

The adsorption studies for the evaluation of the isotherms were conducted in the SCPS and the MCPS. The Langmuir and Freundlich were used to study both systems, while the extended Langmuir (EL), the modified competitive Langmuir (MCL) and the Sheintuc-Rebhun- Sheindorf (SRS) were applied to study the MPS. The parameters are represented in Table 4 (a-c), and the plots are shown in Fig. 5(a-i). The parameters of the isotherms were determined from the non-linear forms of the isotherms, as represented in equations 6 to 11, and these were solved using the Excel solver ad-ins by trial and error iteration.

1. Langmuir model: this is expressed as:

$$q_e = \frac{K_L C_e q_{max}}{1 + K_L C_e} \quad (6)$$

2. Freundlich model is given as:

$$\log q_e = K_F C_e^{1/n} \quad (7)$$

Where, q_e = equilibrium adsorption capacity (mg/g); C_e = equilibrium concentration (mg/l); q_m = maximum adsorption capacity predicted by Langmuir model (mg/g); and K_L = Langmuir constant (Ayewei *et al*., 2017; Kaveeshwar *et al*., 2018). Also K_F = adsorption capacity; and n = adsorption intensity. When 0 > n > 1, this implies favourable adsorption conditions (Xu *et al*., 2015)

The coexistence of contaminants in aqueous solution could result in an increase, decrease or absence of interface in the adsorption efficiency of the adsorbent. One of the methods of studying the interactions of these pollutants is by finding the ratio of the adsorption capacity of the different pollutants in the multiple components system (Q_{MPS}) to their adsorption capacity (Q_{SPS}) in single component systems.

Three types of effects are demonstrated by the multi-component system and they are as follows:

- qm_{MPS} / qm_{SPS} > 1; synergy exists, adsorption of contaminant increases in the presence of other pollutants**.**
- qm_{MPS}/ qm_{SPS} = 1; non-interactive, there is no interaction between the pollutants
- qm_{MPS} / q_{SPS} <1; Antagonistic, adsorption of pollutants decreases in the presence of other pollutants (Neris *et al*., 2019 [9]; Yadav *et al*., 2021) [20].

The presence of multiple pollutants in waste water will lead to competition and interaction among the pollutants the single component isotherm models are adapted to multi-component systems, to account for the change in adsorption mechanisms (Girish, 2017) [4].

1. The non-modified Langmuir isotherm model is represented as:

$$q_{e,i} = \frac{q_{m,iK_L,i_{c_e,i}}}{1 + \sum_{\bar{J}=}^{N} 1^{b_{L,\bar{j}} c_{e,J}}} \quad (8)$$

2. Modified Competitive Langmuir Isotherm (MCL)

$$q_e = \frac{q_{m,i} K_{L,i} (Ce, i/\eta_{L,i})}{1 + \sum_{J=1}^{N} K_{L,J} \left({}^{C_{e,J}} / _{\eta_{L,J}} \right)} \quad (9)$$

The Sheindorf–Rebuhn–Sheintuch (SRS) model is the modified form of the Freundlich isotherm in MPS

$$q_{e,i} = K_{F,1} \sum_{J=1}^{N} (\alpha_{ij} C_{e_i})^{1/n_i - 1} \quad (10)$$

η_L, = interaction factor which is dependent on the concentration of other components (Gupta and Balomajumder, 2015) [5]. α_{ij} = the competition coefficient which describes the inhibition of the adsorption of component i by j (Zhang, *et al*., 2016) [23]**.**

In addition to R^2, the average relative error (ARE) and the sum of squares err0 (SSE) given equations 10 and 11 were used to confirm the fitness of the isotherms models to experimental data. These results are further validated by the closeness of the qe(exp) vs Ce to qe(calc) vs Ce plots.

$$\text{ARE} = \frac{100}{n} = \sum_{-i=1} \left| \frac{q_{e,cal} - q_{e,cal}}{q_{e \notin x_P}} \right| \quad (11)$$

$$\text{SSE} = \sum_{i=1}^{n} (q_e\, exp - q_e calc)^2 \quad (12)$$

With R^2 (0.9984-0.9999) values which are very close to unity, and the coincidence of the qe(cal)-Ce plots to the $qe_{(exp)}$-Ce plots, all the extended isotherm models provided good fits for the experimental data of the adsorption of Pb^{2+} on T-BC500 in the MPS, but the best fitting isotherm model is the MCL The results for the adsorption of Cu^{2+} showed that SRS (R^2 = 0.9739) and NMCL (R^2 = 0.9999) proved to be best fitted to the experimental data of its adsorption. Despite the high R^2 (0.9999) value of the MCL isotherm, it was not considered because of the shift of the qe(calc)-Ce plots from that of $qe_{(exp)}$-Ce. The SRS was the best correlated to the experimental data as demonstrated by the plots and R^2 value (0.9500) for the adsorption of phenol on T-BC500. The qm of the NMCL were 382.84, 1449.21, and 8503.28mg/L, and of the MCL they were 382.24, 671,95 and 226.19 for Pb^{2+}, Cu^{2+} and phenol respectively. The values of η for the MCL isotherm models indicated that Cu^{2+} (η = 71.39) suppressed the adsorption of Pb^{2+} (η = 8.02) and phenol (η = 7.66) in the MPS, and this accounts for its high value of qm.

The use of the Langmuir and Freundlich isotherms to model the adsorption of the pollutants in MPS showed that they were both well fitted to the experimental data of the adsorption of Pb^{2+} Cu^{2+} and phenol in MPS. However, the R^2 (0.9999) of the Langmuir was higher than that of Freundlich (R^2=0.9996) for Pb^{2+} making it a better choice. The Freundlich model with a higher R^2-0.9990 for Cu^{2+} provided a better fit for its adsorption. the values of n > 1 show favourable adsorption. The $\mathbf{q_{mMPS}/q_{mSPS}}$ values were > 1 for all the components, this indicates the existence of synergy among the pollutants and thus the increased adsorption capacities were increased.

From the R^2 values, the error functions, and the qe vs Ce plots, the Freundlich isotherm provided the best fit for the experimental data of the adsorption of Pb^{2+} (R^2= 1.00), Cu^{2+}

(R^2=0.996) and phenol (R^2= 1.00) in the SPS. 1/n values for Pb^{2+} and Cu^{2+} were 0.42 and 0.25 respectively, showing favourable adsorption and it was for phenol, which suggested irreversible adsorption.

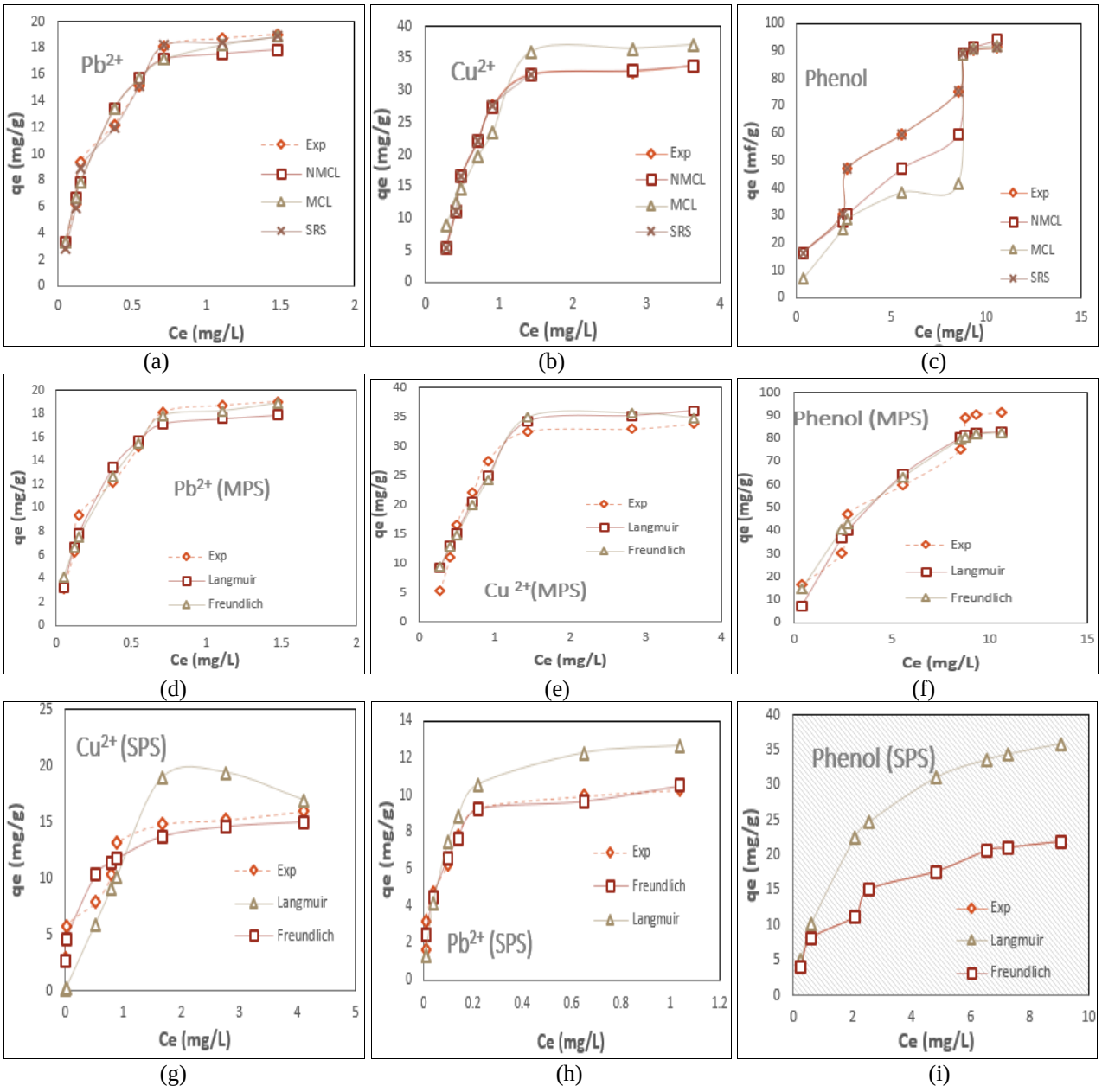

Fig 3: Non-linearised isotherm plots: (a-c). non-modified isotherms of pollutants in MPS; (d-f). modified isotherms of pollutants in MPS; (g-i). non-modified isotherms of pollutants in SPS

Table 4: Modified isotherm model parameters for adsorption of Pb2+, Cu2+ and phenol on T-BC in MCS

Isotherm/Parameter/Adsorbates	Pb(II)	Cu (VI)	Phenol
NMCL			
q_m (mg/g)	382.82	1449.21	8503.28
KL (L/mg)	0.04	0.001	0.0001
R^2	0.9999	0.9996	0.9723
ARE	0.01	0.01	2.90
SSE	0.0013	0.004	47.00
Modified competitive Langmuir			
q_m (mg/g)	382.84	627.95	225.19
K_L (L/mg)	1.90	1.92	0.67
ŋ	8.02	71.39	7.66
q_{mMPS}/q_{mSPS}	22.15		
R^2	0.9996	0.9999	0.9790
ARE	0.02	0.025	4.62
SSE	$1.32x10^{-5}$	$1.38x10^{-5}$	0.0061
Sheindorf–Rebuhn–Sheintuch (SRS)			

K_F (L/mg)$_F$	13.05	16.37	61.05
1/n	0.00	0.00	0.0
a	1.02	1.06	1.008
R^2	0.9984	0.9439	0.9500
ARE	1.27	3.52	0.007
SSE	2.24	7.34	0.002

Table 4 (b): Non-modified Isotherm model parameters of the adsorption of Pb2+. Cu2+ and Phenol on T-BC500 in MPS

Isotherm/Parameter/Adsorbates	Pb(II)	Cu (VI)	Phenol
Langmuir			
q_m (mg/g)	25.22	98.69	151.45
K(L/mg)	2.99	0.37	0.13
q_{mMPS}/q_{mSPS}	1.62	2.39	3.44
R^2	0.9999	0.9968	0.9947
ARE	0.01	0.27	0.40
SSE	0.01	3.81	0.55
Freundlich			
K_F (L/mg)	21.57	26.21	24.99
1/n	0.55	0.80	0.54
R^2	0.9997	0.9990	0.9986
ARE	0.05	0.17	0.17
SSE	0.04	1.56	11.13

Table 4(c): Isotherm model parameters of the adsorption of Pb^{2+}. Cu^{2+} and Phenol on T-BC in SPS

Isotherm/Parameter/Adsorbates	Pb(II)	Cu^{2+}	Phenol
Langmuir			
q_m (mg/g)	16.15	41.52	43.56
K(L/mg)	8.53	0.27	0.51
R2	0.9880	0.9397	0.9970
ARE	0.93	16.4	0.06
SSE	0.3.53	4.26	0.85
Freundlich			
K_F (L/mg)$_F$	17.66	12.09	10.21
1/n	0.42	0.25	1.00
R^2	1.00	0.9996	1.00
ARE	0.003	0.34	$2.76x10^{-6}$
SSE	$3.76x10^{-5}$	0.15	$1.62x10^{-5}$

Table 5: Thermodynamics Parameters of Pb^{2+}. Cu^{2+} and Phenol on T-BC in MPS

Pollutant	T K	$\Delta H°$ kJmol^{-1}	$\Delta S°$ K^{-1} Jmol^{-1}	ΔG^o kJmol^{-1}	R^2
Pb^{2+}	298	68.45	255.747	-8.02	0.9549
	308			-9.76	
	318			-13.18	
Cu^{2+}	298	14.43	74.35	-7.74	0.9957
	308			-8.43	
	318			-9.22	
Phenol	298	15.84	72.40	-5.74	0.9964
	308			-6.42	
	318			-7.20	

Thermodynamics of the adsorption process

The effect of temperature on the adsorption of Pb^{2+}, Cu^{2+} and phenol on T-EB400 was conducted at 25,35 and 45 ^oC. the negative values of ΔG^o are attributable to the spontaneity of the process and increase with increasing temperature as depicted by the rising negativity of $\mathbf{\Delta G^o}$ with temperature. The positive values of $\Delta H°$, which were 68.45, 14.43 and 15.84kJmol^{-1} for Pb^{2+}, Cu^{2+} and phenol respectively are attributable to the endothermic nature of the adsorption process and the adsorption efficiency which increased with temperature. The possible reason for this could be that the hydrated outer layers of the adsorbent were dehydrated to a certain extent due to the presence of dissolved ions in the solution, resulting in the endothermic heat of dissolution being greater than the exothermic heat of adhesion to the surface of the alginate (Deng *et al*., 2017). Also, the positive values of $\Delta S°$ suggest that the degrees of freedom increased at the solid–liquid interface during the adsorption process. The resulting increase in randomness in the system which occurs as the process progressed resulted from the displacement of the coordinated water molecules by metal cations and organic molecules.

Conclusion

Green low-cost tri-composite kaolin-plantain pseudo-stem-snail shell biochar was developed for the removal of mixed pollutants in wastewater. The characterization of the T-BC showed the carbon content decreased with temperature, and increased surface functional groups due to the presence of diverse constituents. Removal efficiencies of T-BC500 were 100, 91.2 and 80.14% for Pb^{2+}, Cu^{2+} and phenol respectively. The adsorption of Pb^{2+} and Cu^{2+} increased with pH up to pH 6, while that of phenol remained relatively constant with pH. The phenomenon implied that the adsorption of Pb^{2+} and Cu^{2+} may have occurred by ion exchange and chemisorption, while that of phenol occurred by molecular movements through van der Waals forces. The adsorption of the components was enhanced in the MPS as compared to the SPS. This means that the presence of other pollutants had a synergistic effect on the adsorption of each pollutant. The interactive factor showed that Cu^{2+} suppressed the adsorption capacity of Pb^{2+} and phenol. The synthesized tri-composite biochar has shown excellent characteristics for environmental sequestration.

Conflicts of interest

Authors confirm that the is no conflict of interest

Acknowledgment

The authors wish to acknowledge the support of Prof Jean. Mulopo of the School of Chemical Engineering, University of the Witwatersrand, Johannesburg, South Africa for the use of his laboratory.

References

1. Arif M, Liu G, Yousaf B, Ahmed R, Irshad SA, Zaidi-ur-Rehman M, Muhammad S. Synthesis, characteristics and mechanistic insight into the clays and clay minerals-biochar surface interactions for contaminants removal-A review. J Clean Prod,2021:310.
2. Belhouchat N, Zaghouane-Boudiaf H, Viseras C. Removal of anionic and cationic dyes from aqueous solution with organo-bentonite/sodium alginate encapsulated beads. Appl Clay Sci,2017:135:9-15.

3. Dai L, T. F., Li H, Zhu N, He M, Zhu Q, *et al*. Calcium-rich biochar from the pyrolysis of crab shell for phosphorus removal. J Environ Manage,2017:198:70-74.
4. Girish C. Various Isotherm Models for Multicomponent Adsorption: A Review. Int J Civil Eng Technol,2017:10:80-86.
5. Gupta A, Balomajumder C. Simultaneous removal of Cr(VI) and phenol from binary solution using Bacillus sp. immobilized onto tea waste biomass. J Water Process Eng,2015:6:1-10.
6. Jianga X, Ruib H, Chena G, Xing B. Facile synthesis of multifunctional bone biochar composites decorated with Fe/Mn oxide micro-nanoparticles: Physicochemical properties, heavy metals sorption behaviour and mechanism. J Hazard Mater,2020:399:123067.
7. Kooh M, Lim L, Dahri M. LAzolla pinnata, an efficient low-cost material for the removal of methyl violet 2B by using adsorption methods. Waste Biomass Valoriz,2015:547-559.
8. Lalhmunsiama D. T.-M. Surface-functionalized activated sericite for the simultaneous removal of cadmium and phenol from aqueous solutions: Mechanistic insights. Chem Eng J, 2015. doi:http://dx.doi.org/10.1016/j.cej.2015.08.072.
9. Neris J, Luzardo F, da Silva E, Velasco F. Evaluation of adsorption processes of metal ions in multi-element aqueous systems by lignocellulosic adsorbents applying different isotherms: a critical review. Chem Eng J,2015:357:404-420.
10. Nhung N, Long V, Fujita T. A critical review of snail shell material modification for applications in wastewater treatment. Materials,2023:16(095). doi:https://doi.org/10.3390/ma16031095.
11. Oladoja N, Adelagun R, Ahmad A, Olalade A. Phosphorus recovery from aquaculture wastewater using thermally treated gastropod shell. Process Saf Environ Prot,2015. doi:http://dx.doi.org/10.1016/j.psep.2015.09.006.
12. Paithankar J, Saini S, Dwivedi S, Sharma A, Chowdhuri D. Heavy metal associated health hazards: An interplay of oxidative stress and signal transduction. Chemosphere,2021:267.
13. Parveen S, Chakraborty D, Chanda S, Barik P. Microstructure Analysis and Chemical and Mechanical Characteristics of the Shells of Thee Freshwater Snail. ACS Omrga,2020:5:25757-25771.
14. Popoola L. Characterization and adsorptive behaviour of snail shell-rice husk (SS-RH) calcined particles (CPs). Helyon, 2019. doi:10.1016/j.heliyon.2019.e01153.
15. Premarathna K, Rajapakshaa A, Adassoriya N, Sakar B, Sirimuthu N, Cooraye A, *et al*. Clay-biochar composites for sorptive removal of tetracycline antibiotic in aqueous media. J Environ Manage,2019:238:315-322.
16. Qu J, Dong M, Wei S, Meng Q, Hu L, Hu Q, *et al*. Microwave-assisted one-pot synthesis of β-cyclodextrin modified biochar for concurrent removal of Pb(II) and bisphenol a in water. Carbohydr Polym,2021:250:117003.
17. Prihatdini RR, Suratman A, Siswanta D. Linear and nonlinear modeling of kinetics and isotherm of malachite green dye adsorption to trimellitic-modified pineapple peel. Mater Today Proc,2023:88:33-40.
18. Wang H, Gao B, Fang J, Ok O, Xuea G, Yanga K, *et al*. Engineered biochar derived from eggshell-treated biomass for aqueous lead. Ecol Eng, 2017. doi:http://dx.doi.org/10.1016/j.ecoleng.2017.06.029.
19. Wang X, Gu Y, Tan X, Liu Y, Zhou Y, Hu X, *et al*. Functionalized BC/clay composites for reducing the bioavailable fraction of arsenic and cadmium in river sediment. Environ Toxicol Chem,2019:30:2337-2347.
20. Yadav S, Yadav A, Bagotia S, Sharma A, Kumar S. The adsorptive potential of modified plant-based adsorbents for sequestration of dyes and heavy metals from wastewater - A review. J Water Process Eng,2021:42:102148.
21. Yao Y, Gao B, Fang J, Zhang M, Chen H, Zhou Y, *et al*. Characterization and environmental applications of clay–biochar composites. Chem Eng J,2014:242:136-143.
22. Zhang J, Wu C, Hou W, Zhao Q, Liang X, Xin S, *et al*. Biological calcium carbonate with a unique organic–inorganic composite structure to enhance biochar stability. Environ Sci: Processes Impacts, 2021, 1747.
23. Zhang L, Wei J, Zhao X, Li F, Jiang F, Zhang M, *et al*. Competitive Adsorption of Strontium and Cobalt onto Tin Antimonate. Chem Eng J,2016:265:679-689. doi:DOI:10.1016/j.cej.2015.10.
24. Zhang W, Ou J, Wang B, Wang H, He Q, Song J, *et al*. Efficient heavy metal removal from water by alginate-based porous nanocomposite hydrogels: The enhanced removal mechanism and influencing factor insight. J Hazard Mater, 2023, 418.
25. Zhuang Y, Yu F, Chen H, Zheng J, Ma J, Chen J. Alginate/graphene double-network nanocomposite hydrogel beads with low-swelling, enhanced mechanical properties, and enhanced adsorption capacity. J Mater Chem A,2016:4:10885–10892.